論文 / 著書情報
Article / Book Information

Title	Strength of bolted steel structural members under eccentric tension
Authors	Kazuma Nagasato, Kikuo Ikarashi, Kazuya Mitsui
Citation	Japan Architectural Review, Vol. 6, Issue 1,
Pub. date	2023, 10
DOI	https://doi.org/10.1002/2475-8876.12409
Creative Commons	Information is in the article.

Japan Architectural Review
Open Access
Architectural Institute of Japan

Translated Paper

Strength of bolted steel structural members under eccentric tension

Kazuma Nagasato, Kikuo Ikarashi and Kazuya Mitsui

Department of Architecture and Building Engineering, Tokyo Institute of Technology, Tokyo, Japan

Correspondence
Kazuya Mitsui, Department of Architecture and Building Engineering, Tokyo Institute of Technology, Tokyo, Japan.
Email: mitsui.k.ad@m.titech.ac.jp

Funding information
JSPS KAKENHI, Grant/Award Number: JP20H2294

The Japanese version of this paper was published in volume 86, number 789, pages 1570–1580, https://doi.org/10.3130/aijs.86.1570, of the *Journal of Structural and Construction Engineering (Transactions of AIJ)*. The authors have obtained permission from the editor of the *Journal of Structural and Construction Engineering (Transactions of AIJ)* for secondary publication of the English version in another journal. This paper is a translation of the original Japanese version with slight modifications and corrections.

Received January 1, 2023; Accepted September 24, 2023

doi: 10.1002/2475-8876.12409

Abstract

The effective cross-sectional area method for the outstanding leg is utilized as an ineffective area to evaluate the strength in the present Japanese design standard. Given that this evaluation method is fundamentally premised on experimental outcomes derived from relatively thick plates, it must be extended to brace members composed of thin plates. In this study, we conduct bolt joint experiments and numerical analyses on thin-plate angles and channel members, with the aim to elucidate the elements influencing the efficiency of the joint. We propose a unified bolt joint strength evaluation formula that also considers thin-plate members.

Keywords
angle member, bolted connection, connection efficiency, connection strength, eccentric connection

1. Introduction

Low-rise steel-framed structures providing ample space are intended to serve as disaster recovery facilities because of their high accommodation capabilities and must have high seismic resilience to serve as a base of operations. In these low-rise steel-framed structures, columns are often constituted by I-shaped steel members and bracing systems are generally deployed in minor axial directions. Braces are structurally important members that resist seismic loads. Their resistance in connections significantly affects the behavior and resistance of the moment frame, including the bracing. Therefore, the brace connections must be ensured to not rupture until the structural components that make up the frames undergo plastic deformation. In the course of catastrophic seismic events, such as the Miyagi earthquake[1] in 1978 and the Kobe earthquake[2] in 1995, significant damage occurs within the moment frame braces, the majority of which is concentrated in braces consisting of a single member with a relatively small cross-sectional profile of the angle members. The damage inflicted by these earthquakes has instigated research[3,4] into the brace systems of angle and channel members.

When a brace comprising a single-angle or single-channel member is subjected to tensile force, eccentricity arises at the connection owing to the lack of biaxial symmetry in these cross sections. Consequently, the designer must consider the moment engendered by the eccentricity. The present Japanese design standard[5,6] provides an equation for the tensile strength of the bolted brace connection, which disregards this moment caused by eccentricity. Instead, it applies a simplified method where a cross section of the outstanding leg is deemed an invalid area, depending on the number of bolts. The invalid cross section of the outstanding leg is statistically derived from the experimental tests conducted by Tanuma et al.,[3,4] utilizing relatively thick equal leg angles with a thickness of 6.0 mm or more. This is then defined as the invalid length[5–7] (h_n) of the outstanding leg, thus resulting in the cross section becoming invalid, as presented in Table 1. According to the Japanese design standard[5,6] steel plates with a thickness of 6.0 mm or more are classified as thick plates, whereas those with a thickness <6.0 mm are categorized as thin plates. However, previous studies[3,4] have not investigated whether the invalid outstanding leg length in Table 1 can be applied to thin-plate members with a thickness of 6.0 mm or less, or to unequal

TABLE 1 Invalid outstanding leg length[5–7] h_n

Number of bolts n	1	2	3	4	5
For angle	$h-t$	0.70h	0.50h	0.33h	0.25h
For channel	$h-t$	0.70h	0.40h	0.25h	0.20h

angle members. Recently, the demand for thin-plate members in steel structures has surged owing to the enhanced efficiency and reduced weight of member cross sections, thus highlighting the importance of investigating the connections of thin-plate members. Contrastingly, numerous experimental studies[8–11] have focused on the shear lag in bolted connections. For instance, Munse et al.[8] noted that shear lag causes nonuniform stress distribution in the single-plane tension connection and that the out-of-plane eccentricity at the connection and the length of the connection significantly influence this. The design equation in the AISI standard,[12] which assumes a reduction in the tensile strength of the brace connection owing to shear lag, is employed to calculate the necessary tensile strength of a connection.

In this paper, plate thicknesses of 6.0 mm or less are defined as thin-plate members, and plate thicknesses thicker than 6.0 mm are defined as thick-plate members, in accordance with the Japanese design standard.[5,6] This study aims to clarify the factors pertaining to cross-sectional shape that influence the tensile strength of bolted connections in braces. These braces, composed of asymmetric thin-plate members (such as angle and channel members) are frequently employed in steel structures. Therefore, we performed uniaxial tensile tests and finite element analyses (FEA) of bolted connections. Furthermore, we proposed consolidated design equations for assessing the required tensile strength of bolted connections in braces, determined by net section failure, including both thin-plate and thick-plate members. For this purpose, Section 2 discusses the execution of uniaxial tensile tests on brace members with thin-plate asymmetric cross-sectional geometry, to discern the geometric variables influencing the tensile strength of bolted connections. Section 3 assesses the validity of equations employed in Japan and overseas for evaluating the tensile strength of bolted connections. Section 4 includes FEAs to clarify the factors associated with the cross-sectional shape that affect the tensile strength of the connections. Finally, Section 5 proposes unified equations for evaluating the tensile strength of bolted connections in braces, applicable to both thin-plate and thick-plate members.

2. Uniaxial Tensile Tests on Eccentrically Connected Thin-Plate Braces

2.1 Configuration and test setup

Herein, uniaxial tensile tests of bolted connections were performed on asymmetric thin-plate members to determine the cross-sectional shape-related factors influencing the tensile strength of bolted connections. The specimens' dimensions are displayed in Figure 1, a schematic of the specimens is provided in Figure 2, and the definitions of the symbols are listed in Table 2.

The experimental test parameters included the thickness of the specimen (t), outstanding leg length (h), bolt hole diameter

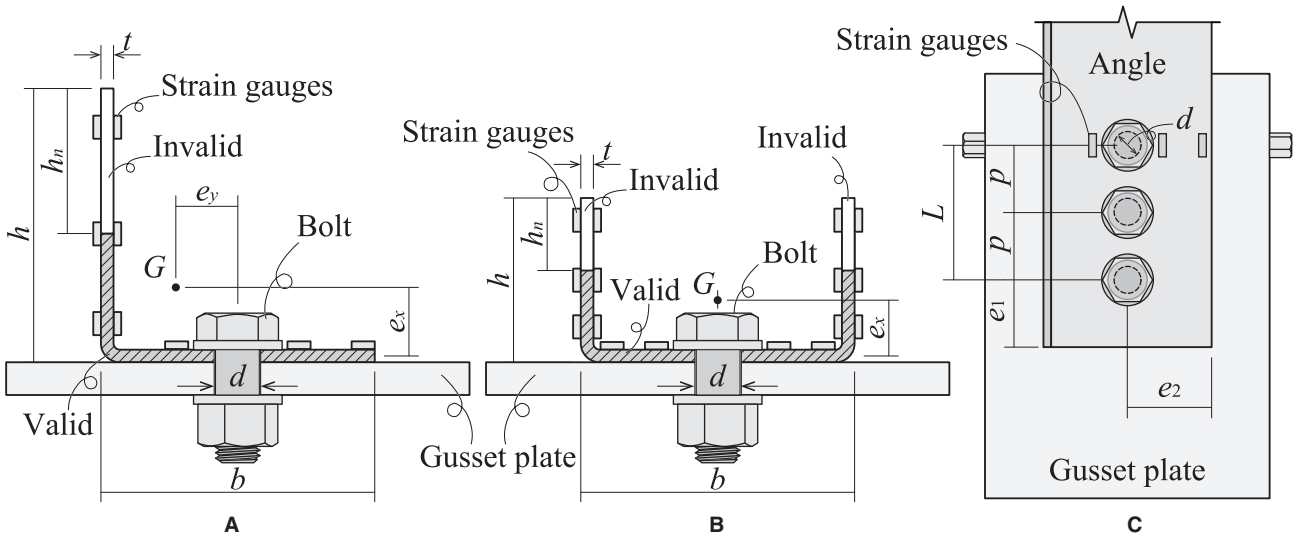

FIGURE 1 Details of the bolted connections of the brace specimen with an asymmetric cross-section: (A) angle member, (B) channel member, and (C) detail of the bolted connection

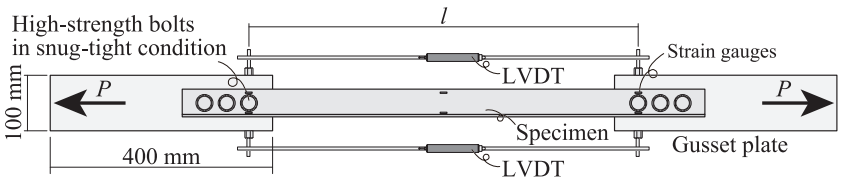

FIGURE 2 Overview of the specimen and test setup

TABLE 2 Symbols used in this study

L: Length of connection [mm] (= $p(n-1)$)	l: Length between first bolts [mm]
t: Thickness [mm]	A_n: Net area [mm^2]
t_{GP}: Thickness of gusset plate [mm]	n: Number of bolts [−]
h: Outstanding leg length [mm]	h_n: Invalid outstanding leg length [mm]
e_1: Edge distance [mm]	e_2: Bolt edge distance [mm]
e_y: Out-of-plane eccentric distance [mm]	e_x: In plane eccentric distance [mm]
p: Distance between bolt holes [mm]	d: Diameter of bolt hole [mm]
$P_{y,e}$: Yield strength obtained via tests [kN]	$P_{u,e}$: Ultimate strength obtained via tests [kN]
P_u: Calculated ultimate tensile strength without considering the invalid length of the outstanding leg [kN] (= $A_n\sigma_u$)	$P_{u,c}$: Calculated ultimate tensile strength considering the invalid length of outstanding leg [kN] (=$(A_n - h_n t)\sigma_u$)
E: Modulus of elasticity [N/mm^2]	ν: Poisson's ratio [−]
σ_y: Yield stress [N/mm^2]	σ_u: Tensile stress [N/mm^2]
ε_y: Strain at yield stress [%]	ε_u: Strain at tensile stress [%]

(d), number of bolts in the longitudinal direction (n), length of the connection (L), edge distance in the direction of the tensile force (e_1), bolt edge distance perpendicular to the direction of the tensile force (e_2), cross-sectional geometry, gusset plate thickness (t_{GP}), and length between the first bolts (l). The thickness (t) was selected for members with a thickness of 6.0 mm or less to investigate the tensile strength of bolted connections for thin-plate members. The bolt hole diameter (d) was configured to be 1 mm more than the shank diameter of the bolt, and two types of bolts, M12 and M16, were employed. A single bolt-row arrangement was implemented for the connections, and the number of bolts in the longitudinal direction (n) was 2, 3, or 5. The distance between the bolt holes (p) was set to the minimum distance of 40 mm, as specified in the AIJ Japanese recommendation for design connections in steel structures,[5] and an additional p = 80 mm was prepared for comparison. The edge distance in the direction of the tensile force (e_1) was determined according to the Japanese recommendations,[5] as a function of the number of bolts and bolt shank diameter. For this study, the minimum distance e_1 = 40 mm was considered when using M16 bolts, and another shorter distance e_1 = 30 mm. The cross section of the brace members was set to equal leg angle, unequal leg angle, and channel members. When the angle and channel members are connected eccentrically, the angle member exhibits biaxial eccentricity, whereas the channel member exhibits only uniaxial eccentricity. Thus, the effect of the direction of eccentricity was examined by comparing the results of these cross sections. The gusset plate thickness (t_{GP}) was also included as a variable to verify the effect of the out-of-plane stiffness of the gusset plate on the tensile strength. The length of the specimens varied from 380 to 800 mm, including the length between the first bolts (l). The experimental variables for the specimens are summarized in Table 3. The test specimens were fabricated by combining these experimental variables as required.

The study used 61 specimens; a comprehensive list is available in Appendix A. Most specimens were cold-formed angle and channel members, whereas a few were hot-rolled. Appendix A also includes a list of the coupon test results for the steel used in the tensile tests. High-strength bolts were utilized for the connection of the specimens in snug-tight conditions. The torque was carefully controlled by hand-tightening with a wrench to examine the post-slip tensile strength of the bolts. The bolts were positioned through the centerline of the connected leg, and the size of the bolt hole on the gusset plate was identical to that of the brace members. The measurement plan is depicted in Figure 2. A displacement measuring device, known as a high nut, was welded to the side of the gusset plate to measure the displacement between the first bolt. Two linear variable differential transformers were utilized to measure the elongation between the first bolt holes, and the average elongation (δ) was employed to establish the load–displacement relationship. Strain gauges were installed at the positions indicated in Figures 1 and 2 to monitor the strain distribution along the direction of the tensile force. The tensile test was conducted using an Amsler universal testing machine (capacity, 1000 kN) at the Tokyo Institute of Technology, Tokyo, Japan. A uniaxial tensile load was applied to the specimen throughout the test until the connection fractured.

TABLE 3 Range of experimental variables

t: 1.6, 2.3, 3.2, 4.0, 4.5, 6.0, and 8.0 [mm]	n: 2, 3, and 5
e_1: 30, 40 [mm]	e_2: 25, 40, 50 [mm]
d: 13 for M12, 17 for M16 [mm]	p: 40, 80 [mm]
l: 380, 700, 800 [mm]	t_{GP}: 2t, 3t, 5t

2.2 Deformation of the brace connection

Figure 3 illustrates the relationship between the normalized load (P/P_u) and normalized elongation (δ/δ_u) for each experimental variable. The load (P) on the vertical axis is normalized by the calculated tensile strength (P_u) based on the net area (A_n). The average elongation (δ) is normalized by the elongation (δ_u) at ultimate strength. The $\bigtriangledown$ symbol in Figure 4 indicates the point of yield strength ($P_{y,e}$) as defined in Appendix B. Figure 4 presents the specimen's deformation after testing. First, the specimen's behavior confirmed in the tensile test was described. The ultimate tensile strength of most specimens was determined by the net section failure at the first bolt hole position (Figure 4A). For specimens where net section failure was observed, cracks appeared at positions perpendicular to the stress direction of the first bolt hole. The tensile strength decreased rapidly when the ductile fracture reached the connected leg's edge. Out-of-plane deformations occurred around the connections from the start of loading, eventually reaching the ultimate tensile strength (Figure 4B), around the yield strength $P_{y,e}$. Concurrently with the out-of-plane deformation surrounding the connection, out-of-plane deformations of the connected leg occurred when the specimens consisted of relatively thin plates or large outstanding legs (Figure 4C). These out-of-plane deformations of the cross sections were confined to the region surrounding the connection. No deformation of the cross sections was observed in the center of the specimen, the area most distant from the connections. For a few specimens, the ultimate strength was determined by tear-out failure or block-shear failure.

2.3 Ultimate strength of a bolted connection composed of an asymmetric cross section

The connection efficiency J_m, expressed in Equation (1) as the ratio of the ultimate tensile strength $P_{u,e}$ to P_u, was replaced by the ultimate tensile strength to clarify the factors affecting the tensile strength of the connection.

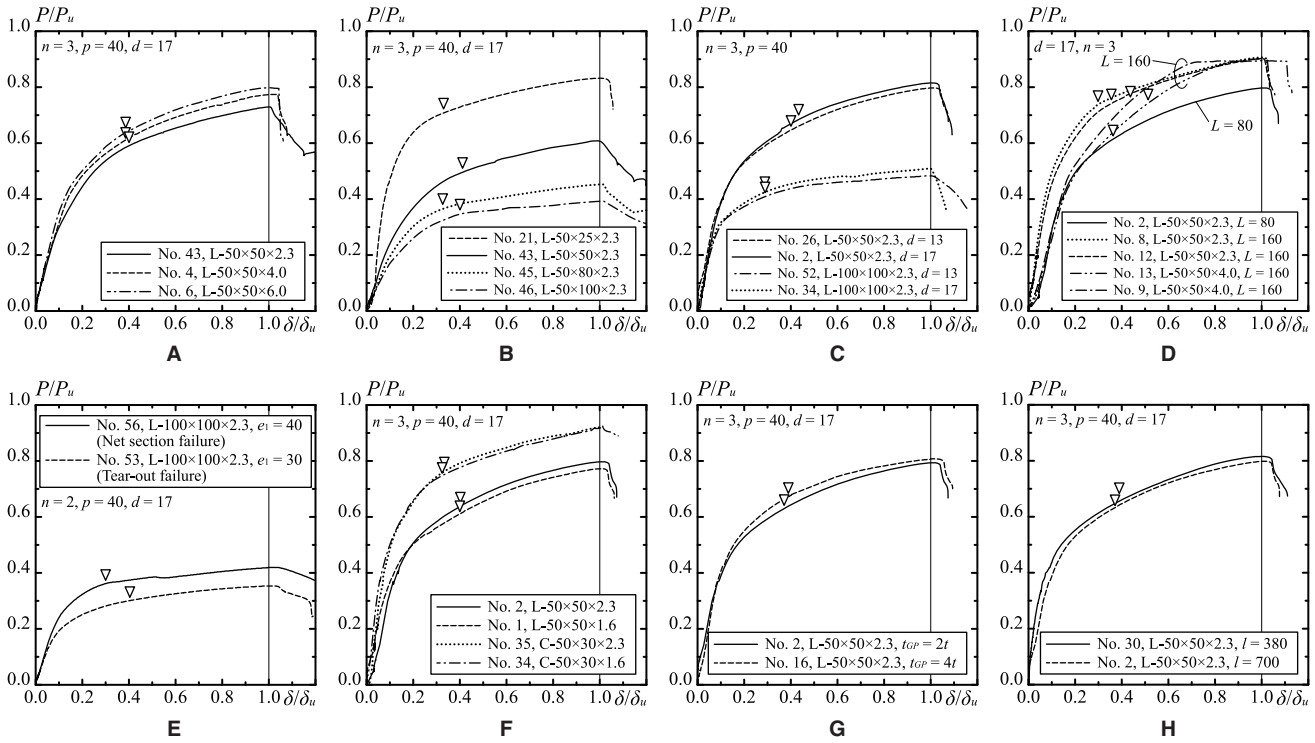

FIGURE 3 Relationship between normalized load P/P_u and normalized elongation δ/δ_u: (A) effect of thickness t, (B) effect of outstanding leg length h, (C) effect of diameter of bolt hole d, (D) effect of connection length L, (E) effect of the edge distance e_1, (F) effect of cross-sectional shape, (G) effect of the gusset plate thickness t_{GP}, and (H) effect of member length l

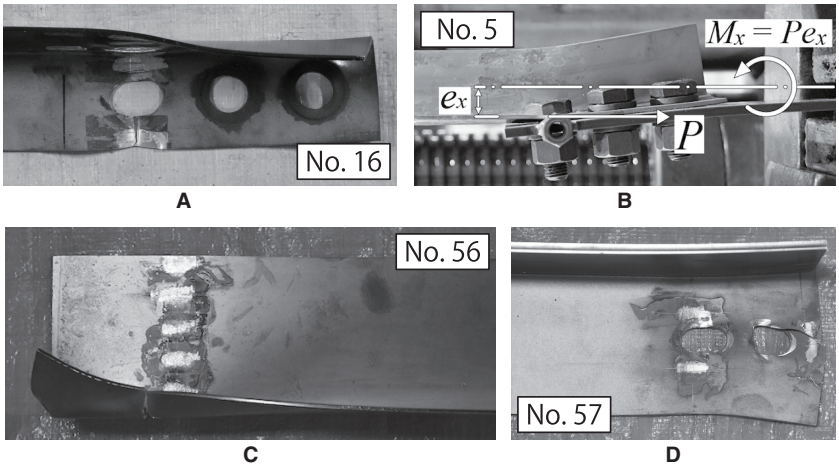

FIGURE 4 Detail of connection failure: (A) net section fracture, (B) eccentric moment at the connection, (C) out-of-plane deformation of the edge, and (D) fracture at end edge

$$J_m = \frac{P_{u,e}}{P_u}. \quad (1)$$

Figure 3A illustrates the effect of thickness (t) on connection efficiency. The thicker the plate across the cross section, the smaller the in-plane eccentricity distance, e_x (Figure 1A). Therefore, the connection efficiency tends to increase with increasing thickness. This result implies that the width-to-thickness ratio affects connection efficiency. Figure 3B shows the effect of the outstanding leg length (h). Connection efficiency decreases as the outstanding leg length increases, thus indicating that the outstanding leg length affects the tensile strength. This phenomenon can be attributed to the increase in eccentricity distance (e_x) stemming from the increase in outstanding leg length. Figure 3C compares the effect of the bolt hole diameter (d). Within the scope of bolt hole diameters explored in this experiment, the effect of the bolt hole diameter on connection efficiency is negligible, regardless of the cross-sectional shape.

Figure 3D examines the impact of connection length (L). Connection length (L), adjusted by modifying the number of bolts (n) and distance between the bolt holes (p), is defined as

the distance from the center of the first bolt hole to the center of the nth bolt hole (Figure 1C). Figure 3D reveals that given an equal connection length (L), the connection efficiency remains relatively uniform, irrespective of variations in the number of bolts and the distance between bolt holes. This suggests that the conventional Japanese standards,[5–7] which determine the ultimate tensile strength of bolted connections based on the number of bolts (n), may not be the most optimal approach. Figure 3E compares the effect of edge distance in the direction of the tensile force (e_1). Specimens with longer edge distances demonstrated higher connection efficiency. Furthermore, the failure type is a function of the edge distance, with a net section fracture (Figure 4A) occurring at e_1 = 40 mm, which satisfies the requirements of the Japanese standard,[5] and a tear-out failure (Figure 4D) occurring at e_1 = 30 mm (which does not meet the requirements). These variations in the nature of failure significantly influence connection efficiency. For the specimens where tear-out failures occurred, cracks appeared in the stress direction of the bolt hole on the edge side; consequently, the tensile strength decreased rapidly when the crack reached the edge. Figure 3F elucidates differences in the cross-sectional shapes. The channel members exhibited a higher connection efficiency than the angle members. This outcome may be attributed to: the uniaxial eccentricity of the channel member, as opposed to the biaxial eccentricity of the angle member, zero eccentricity distance (e_y) (Figure 1B), and the smaller eccentricity distance (e_x) of the channel member compared with that of the angle member. Finally, Figure 3G compares the influence of the gusset plate thickness (t_{GP}). The out-of-plane stiffness of the gusset plates increased with the gusset plate thickness, thus curtailing the out-of-plane deformation surrounding the connections (Figure 4B). However, although the out-of-plane deformation of the gusset plate decreased, the deformation in the angle member remained unchanged. Thus, the connection efficiency stayed consistent, irrespective of variations in gusset plate thickness, given the minimal effect on deformation surrounding the connection. Figure 3H shows the effect of specimen length (l). Despite changes in specimen length, the connection efficiency maintained its consistency as the out-of-plane deformation surrounding the connections remained unaffected.

The findings from the tensile tests indicate that the plate thickness, outstanding leg length, connection length, and cross-sectional shape significantly influence the connection efficiency. Consequently, these aspects should be considered while calculating tensile strength. Among these factors, plate thickness, outstanding leg length, and cross-sectional shape affect the eccentricity distance (e_x). The connection efficiency decreased with increasing eccentricity, thus indicating that eccentricity effects were prominent in cross sections with low connection efficiency and the tensile force was unevenly distributed in the cross section. The strain distribution within the cross section of the first bolt hole is illustrated in Figure 5, showing five load levels. The strain (ε) depicted on each axis was normalized by the strain at yield stress (ε_y), and specimens with varying outstanding leg lengths are presented in Figure 5A,B respectively. The strain distribution was not uniform across the entire cross section, and the edge of the outstanding leg experienced compressive forces rather than tensile forces. Comparing diverse cross-sectional shapes revealed that almost no tensile force was exerted on specimens with larger outstanding legs (Figure 5B). Essentially, the eccentricity distance determines the ineffective length of the outstanding leg that fails to resist tensile forces.

3. Comparison of Yield and Ultimate Strength with the Current Design Equations in the Standards

Next, the experimental test results were compared and validated against the design equations from the Japanese standard[5,7] and the AISI standard[12] for the yield and ultimate tensile strength of connections. Initially, the yield tensile strength ($P_{y,e}$) derived from the experimental results was compared with the calculated value ($P_{y,c}$; Equation (2)) of the yield tensile strength equation provided in the Japanese standard.[5] The yield tensile strength equation in the Japanese standard considers half the length of the outstanding leg as the ineffective length that fails to resist tensile forces, as follows.

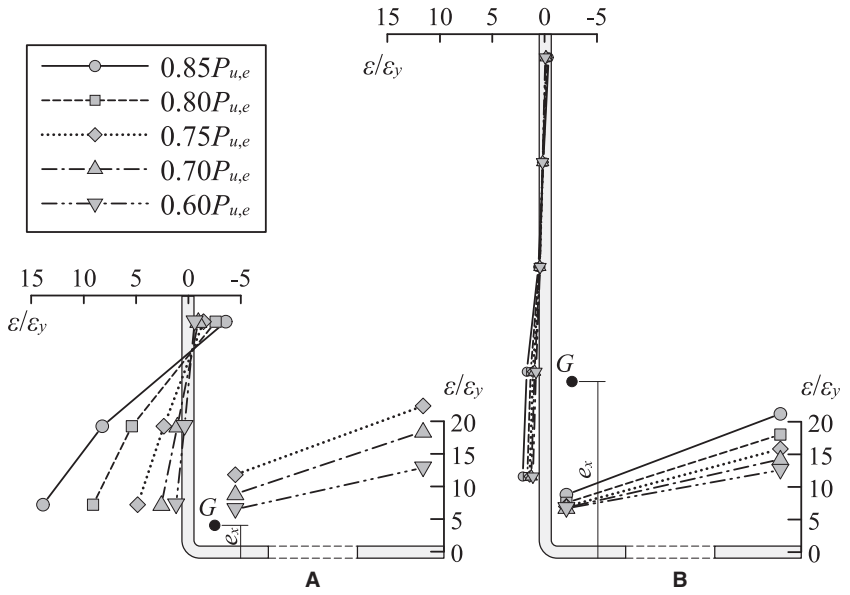

FIGURE 5 Stress distribution in the cross section of the first bolt hole: (A) No. 2 (L-50 × 50 × 2.3) and (B) No. 46 (L-50 × 100 × 2.3)

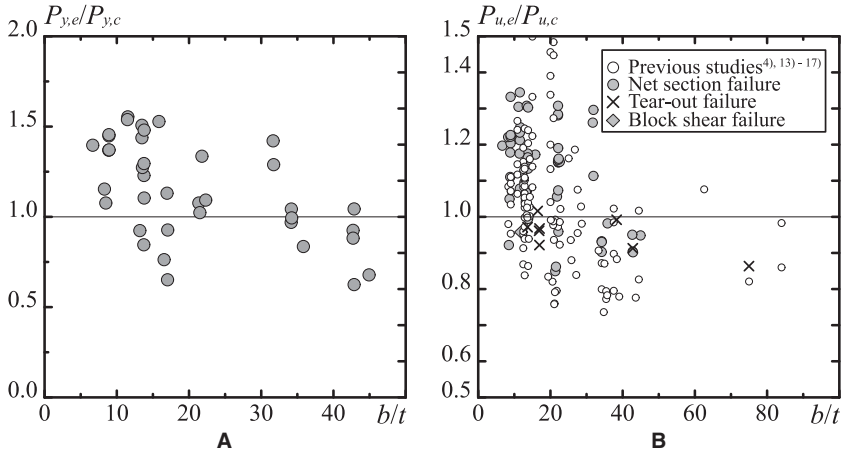

FIGURE 6 Comparison between the test results and design equation of the Japanese standard: (A) yield strength and (B) ultimate strength

$$P_{y,c} = \left(A_n - \frac{h}{2}t\right)\sigma_y. \tag{2}$$

Figure 6A demonstrates a comparison between the experimental outcomes and the calculations grounded on Equation (2). The vertical axis represents the ratio of the calculation results derived from Equation 2 ($P_{y,c}$) to the experimental findings ($P_{y,e}$), whereas the horizontal axis represents the width-to-thickness ratio of the connected legs, b/t. Regardless of the width-to-thickness ratio, the ratio between the calculations and experimental results presented a large scatter, thus implying that the yield tensile strength of the connections is inadequately evaluated in the prevailing Japanese standard. The current calculation for yield tensile strength, as detailed in Equation (2), posits that half the length of the outstanding leg is disregarded, irrespective of the cross-sectional shape. However, Figure 5 reveals that the length of the outstanding leg, subjected to tensile force, varies with the cross-sectional shape. This discrepancy could have contributed to an inaccurate calculation of the yield tensile strength of the connections defined in this study.

The ultimate tensile strength ($P_{u,e}$) obtained experimentally was compared with the calculated value ($P_{u,c}$) in the ultimate tensile strength formula of the existing Japanese standard,[5] depicted in Equation (3). This formula adjusts the invalid length of the outstanding leg (h_n) according to the number of bolts, as outlined in Table 1.

$$P_{u,c} = (A_n - h_n t)\sigma_u. \tag{3}$$

Figure 6B provides a comparison of the experimental findings from this study, previous studies,[4,13–17] and calculations grounded on Equation (3). The vertical axis represents the ratio of the calculation results based on Equation 3 ($P_{u,c}$) to the experimental results ($P_{u,e}$). Specimens marked with x in Figure 6B are those in which the ultimate tensile strength was determined by tear-out failure, while ◇ legend represents block shear failure. They served as reference points owing to differing targeted failure modes. Just as the yield tensile strength (Figure 6A), a large scatter was noted in the ultimate tensile strength, particularly in the range of larger width-to-thickness ratios, where a significant proportion of specimens were found to be unconservative. As discussed in Section 1, the design equations in the existing Japanese standard[5] were formulated based on experiments[3,4] on brace connections with relatively thick (≥6.0 mm) equal leg angles. Consequently, the thinner the plate, that is, the larger the width-to-thickness ratio of the specimen, the less conservative the rating becomes.

Figure 7 compares the experimental results with calculation results based on the design equation for ultimate tensile strength outlined in the Guidebook on Design and Fabrication of High Strength Bolted Connections,[7] expressed as follows.

$$T_n = 3.14A_n\sigma_u\left(1-0.24\frac{1}{n}\right)\left(1-0.64\frac{b-d}{b}\right)\left(1-0.24\frac{e_x}{L}\right)\left(1-0.76\frac{e_y}{L}\right)\left(1-0.12\frac{b}{e_2}\right)\left(1-0.23\frac{h}{b}\right). \tag{4}$$

The vertical axis represents the ratio of calculation results derived from Equation (4) (T_n) to the experimental findings

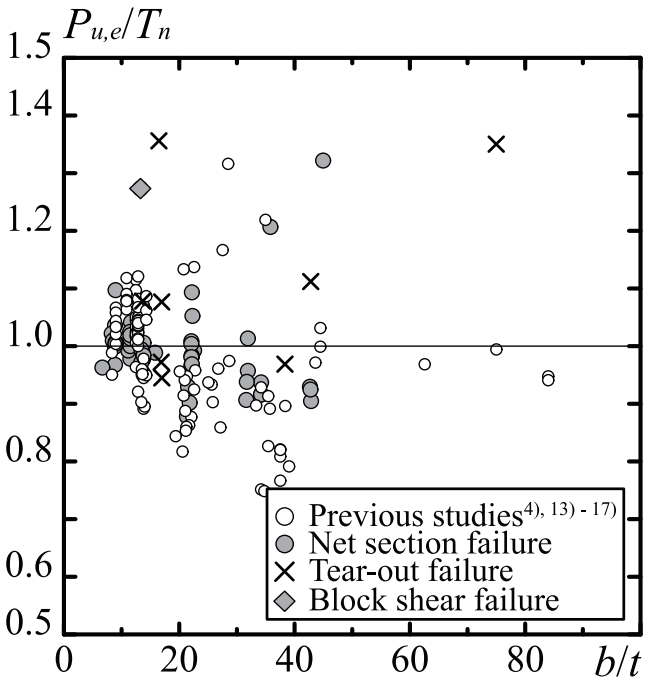

FIGURE 7 Comparison between the test results and design equation in the guidebook on design and fabrication of high strength bolted connections

($P_{u,e}$). Compared with the current Japanese standard[5] (Figure 6B), the scatter becomes small when the width-to-thickness ratio is below 20. However, similar to the current Japanese standard, the number of specimens deemed unconservative increase in the range of larger width-to-thickness ratios.

The 2012 version of the AISI provision[12] provides Equations (5) and (6), in which the ultimate tensile strength of the connections is determined based on the shear lag factor U, the eccentricity distance (e_x) to connection length (L) ratio, and the net area (A_n), which excludes the bolt holes from the gross area. Equation (5) can be utilized for both bolted and welded connections.

$$s_u = UA_n\sigma_u, \tag{5}$$

$$U = \begin{cases} 0.9 & \text{for } 0 \le e_x/L < 0.083 \\ 1-1.2\dfrac{e_x}{L} & \text{for } 0.083 \le e_x/L < 0.50 \\ 0.4 & \text{for } 0.50 \le e_x/L \end{cases}. \tag{6}$$

Figure 8A elucidates the relationship between connection efficiency (J_m) and the e_x/L ratio. The solid line signifies the shear lag factor U, which considers the shear lag effect according to Equation (6). Evidently from the tensile test results of the bolted connection discussed in Section 2, the tensile strength is affected by the eccentricity distance (e_x) and connection length (L). The AISI standard's shear lag factor U comprises these elements and accurately reflects the connection efficiency trend (J_m), which decreases with increasing ratio of e_x/L. Figure 8B compares the calculation results based on the AISI standard design equations (Equations (5) and (6)) with experimental results. The ultimate tensile strength calculated according to the AISI standard design equations yields less scatter compared with the results evaluated in the current Japanese standard. Conversely, as demonstrated in Figures 6B and 7, the proportion of unsafe evaluations increases in the range of larger width-to-thickness ratios, thus decreasing the accuracy of evaluation. A comparison of the 2016 AISI standard's design equations[18] for bolted and welded connections, with the design equations in other design provisions[19,20] is delineated in Appendix C.

The comparisons between calculation results from various design provisions and the tensile test results on brace connections indicate that current design equations tend to yield more conservative evaluations when the width-to-thickness ratio is less than approximately 20. However, as this ratio increases, all evaluation methodologies tend to result in unconservative assessments. Given that bolted connections serve as critical structural elements that withstand seismic loads, the existing equations utilized for calculating tensile strength lack sufficient accuracy. Therefore, a new design equation that comprehensively accommodates both thin and thick members without resulting in unconservative evaluations must be established.

4. Investigation of the Strength of Bolted Connections Using FEA

4.1 Outline of FEA

To elucidate the factors influencing connection efficiency not investigated in the experimental tensile tests described in Section 2, we performed several series of numerical analyses using the versatile finite element (FE) analysis software Abaqus 2019. Figure 9 presents a typical FE model of a bolted connection. This model represents half of the full specimen, taking advantage of its symmetry. The brace member was meshed using a six-node linear continuum element, C3D10. Only contact was considered, whereas friction between components was not considered. The bolt, comprising the bolt head, shaft, and nut, was modeled as a rigid body. As in the experiment, no pretension was applied to the bolts. The minimum mesh size around the first bolt hole, where stress is most concentrated, ranged between $t/2$ and $t/3$ of the plate thickness (Figure 9B,C). The Poisson ratio (ν) was set at 0.3, and the material data implemented in the FE model were the outcomes of the coupon tests conducted in this study. Material data were selected from the test results associated with M tag: b and M tag: i. Table A1 in Appendix A lists the material data used in the FE model, which were chosen based on the plate thickness of the model. All elements followed the von Mises yield criterion and the isotropic hardening law. Figure 9A illustrates the boundary conditions of the FE model. The edge of the gusset plate (A–A section) was presumed to be a fixed support, and rotation of the bolts around the z-axis was restrained. Nodes on the middle cross section (B–B section) were linked to point C—situated at the cross section's center—via rigid links. The load was applied to point C as a tensile force.

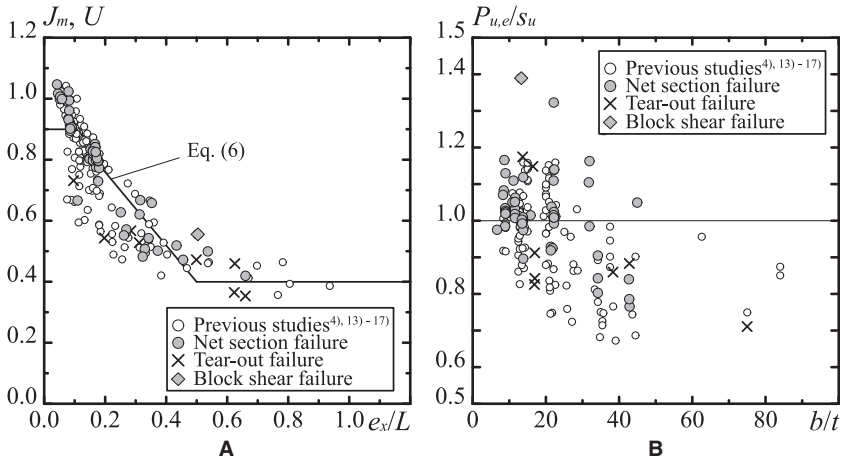

FIGURE 8 Comparisons between test results and design equations in AISI: (A) J_m versus e_x/L and (B) $P_{u,e}/s_u$ versus b/t

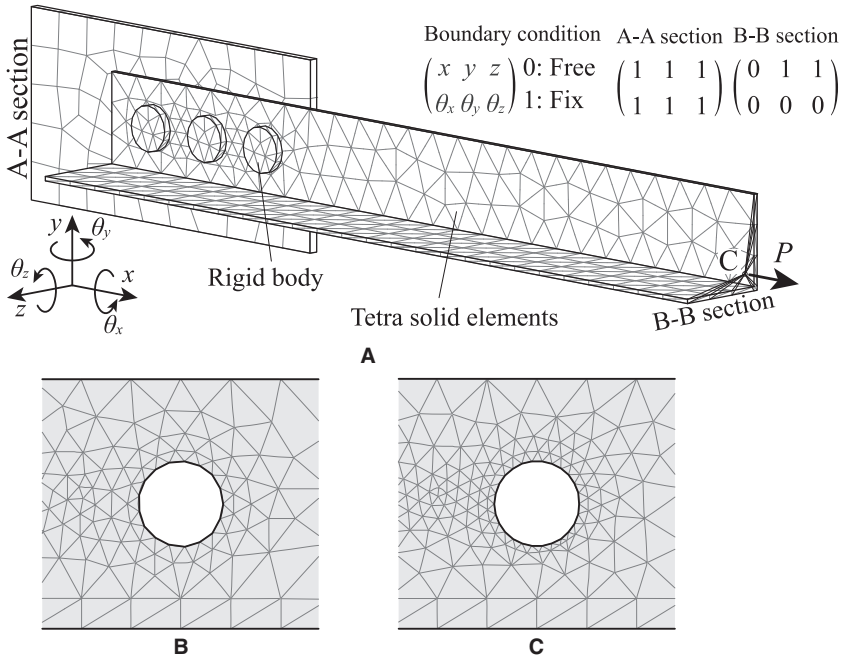

FIGURE 9 Overview of the FE model: (A) half FE model and boundary condition, (B) rough mesh size (minimum size: *t*/2), and (C) fine mesh size (minimum size: *t*/3)

Figure 10 defines the ultimate tensile strength derived from the FEA. It represents the relationship between stress triaxiality (τ) and equivalent plastic strain (ε_{eq}) at nodes surrounding the first bolt hole, where stress is most concentrated. The ultimate tensile strength as determined by FEA ($P_{u,a}$) is defined as the strength at the point where the stress triaxiality-equivalent plastic strain curve (solid line) meets the ductile fracture initiation limit curve[21] (τ_{peak}) as defined in Equation (7):

$$\tau_{peak} = \sqrt{\frac{\varepsilon_u}{\varepsilon_{eq}}}, \tag{7}$$

where τ_{peak} is the ductile fracture limit, ε_u is the strain at the tensile strength, and ε_{eq} is equivalent plastic strain.

Figure 10B provides an example of results obtained by varying the minimum mesh size. The FE model with a minimum mesh size of *t*/3 mm around the first bolt hole demonstrated a better agreement with the ultimate tensile strength obtained from the experiments compared to the model with a minimum mesh size of *t*/2 mm. This confirmation affirms that the method proposed by Totsuka et al.[22] for determining the strength at fracture is adequate for observing the trend in tensile strength. Next, we employed an analytical model with a minimum mesh size of *t*/3 mm.

4.2 Factors affecting bolted connection strength

We examined the influence of bolt hole positions and diameters on the tensile strength of the bolted connections via FEA, aspects which were not assessed in the experimental investigation. Figure 3F indicates that connection efficiency is higher for a channel member than for an angle member. This discrepancy could be attributed to the in-plane eccentricity distance

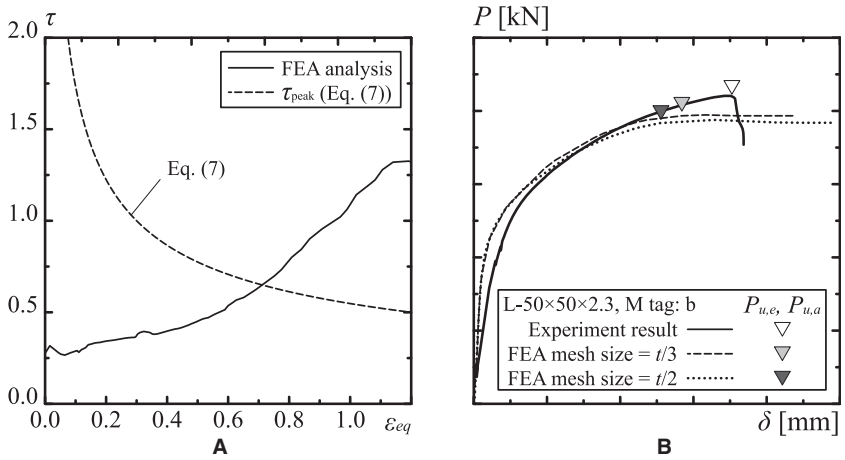

FIGURE 10 Evaluation based on stress triaxiality and equivalent plastic strain: (A) τ versus ε_{eq} around the first bolt hole, and (B) comparison between test results and the FEA results.

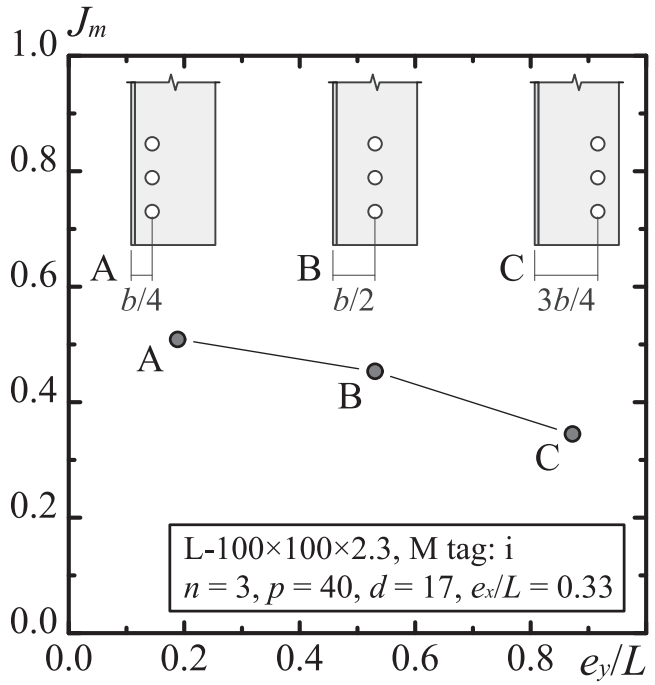

FIGURE 11 Effect of out-of-plane eccentric distance e_y.

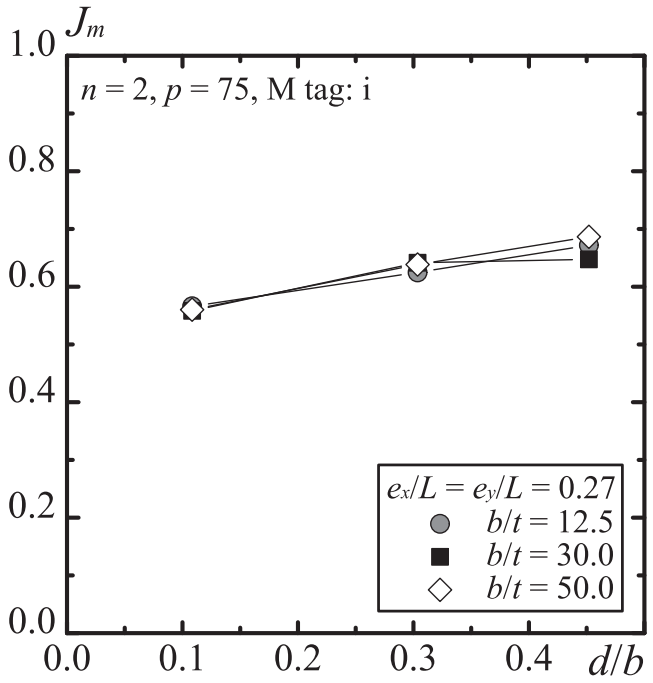

FIGURE 12 Effect of the bolt hole diameter-to-width ratio d/b

(e_y) of the angle member, which contrasts with the zero in-plane eccentricity of the channel member. To investigate the influence of the eccentricity distance e_y, FEA was conducted with varying bolt hole positions while maintaining all parameters constant, except for the eccentricity distance e_y. In this analysis, L-100 × 100 × 2.3 was utilized, and the bolt hole positions were varied for three patterns: $b/4$, $b/2$, and 3 $b/4$ of the connected leg (Figure 11).

Figure 11 presents the effect of the eccentricity distance e_y. The vertical axis represents the connection efficiency (J_m), whereas the horizontal axis represents the ratio between the eccentricity distance and the connection length (e_y/L). Mirroring the J_m–e_x/L relationship shown in Figure 8A, the connection efficiency decreased as e_y/L increased. These results suggest that in addition to the out-of-plane eccentricity (e_x) effect (as confirmed in the experiment), the effect of in-plane eccentricity (e_y) must also be considered when evaluating the connection efficiency.

Next, the effect of the bolt hole diameter was investigated. In the experimental test, bolt hole diameters were set at d = 13 and 17 corresponding to the connected legs of angle members with b = 50 and 100, respectively. The bolt hole diameter to the connected leg ratio varied between d/b = 0.26 to 0.34 and 0.13 to 0.17, which limited a complete understanding of this ratio's influence. In Figure 12, the FE model's cross-sectional shape was modified as necessary to ensure the same eccentricity to connection length ratios (e_x/L and e_y/L), and the ratio of bolt hole diameter to connected leg (d/b) was varied between 0.10, 0.30, and 0.45 to study its impact on connection efficiency. Evidently, the smaller the ratio of the bolt hole diameter to connected leg (d/b), the lower the connection efficiency (Figure 12).

5. Design Equation for Tensile Strength of Bolted Connections of Thin-Plate Structural Members

5.1 Design equation for ultimate tensile strength

Both experimental tensile tests and FEAs demonstrated that the factors influencing the tensile strength of brace connections are the eccentricity distances e_x and e_y, connection length L, and the ratio of the bolt hole diameter to the connected leg d/b. Additionally, the current design equations are inadequate in determining the tensile strength of brace connections. Thus, we proposed unified design equations for the tensile strength of brace connections that accommodate both thin and thick plate members. Evidently, lower eccentricity distances (e_x and e_y) coupled with a larger connection length L results in a higher joint efficiency J_m. The 2012 edition of the AISI shear lag factor U, expressed in Equation (6), considers factors beyond the eccentricity distance e_y in the design equation and approximately captures the trend in connection efficiency. Therefore, we incorporated the effect of the eccentricity distance e_y into the AISI standard's reduction factor.

First, we studied the eccentricity distance between the principal axes and the point where the tensile force acts on the angle member, as shown in Figure 13. Point G represents the cross section's center, and point T is where the tensile force transitions from the bolt to the brace. Given that the principal axes of the angle members are the u and v axes (Figure 13), the effect of eccentric bending must be evaluated using the

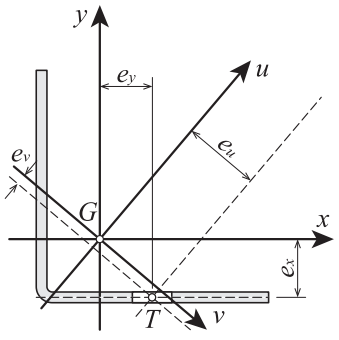

When $e_v = 0$

$$e_u = \sqrt{e_x^2 + e_y^2} = \overline{GT}$$

FIGURE 13 Principal axes of the angle member

eccentricity distances e_u and e_v to properly consider the effect of eccentric bending.

In most of the cross sections used in this experiment, the v-axis, being the principal axis, intersects around point T, where the tensile force is transferred from the bolt to the brace, implying that e_v can be considered approximately zero. The length of the eccentricity distance e_u aligns with the length of GT, as shown in Figure 13, and its length is $\sqrt{e_x{}^2+e_y{}^2}$ due to geometric relationships. In other words, eccentricity distances e_x and e_y, which affect the joint's tensile strength, can be simultaneously considered with the eccentricity distances e_u and e_v by using this length GT. Figure 14A depicts the relationship between connection efficiency and experimental results. The shear lag factor U', proposed in this study, was determined with the AISI standard's shear lag factor U as a reference.

$$U' = \begin{cases} 1-1.2\dfrac{\sqrt{e_x{}^2+e_y{}^2}}{L} & \text{for } 0.0 \le \sqrt{e_x{}^2+e_y{}^2}/L < 0.50 \\ 0.4 & \text{for } 0.50 \le \sqrt{e_x{}^2+e_y{}^2}/L \end{cases}. \quad (8)$$

The shear lag factor U', as denoted in Equation (8) reflects the trend of experimental results and exhibits a smaller variation compared with that demonstrated in Figure 8. This suggests that employing the eccentricity distance to the principal axis as $\sqrt{e_x{}^2+e_y{}^2}$ is effective for arbitrary cross sections. Figure 14B further illustrates the relationship between the width-to-thickness ratio (b/t) and the experimental results, which are based on the ultimate tensile strength S_u' calculated using the shear lag factor U' as given in Equation (9).

$$S_u' = U'A_n\sigma_u. \quad (9)$$

Compared with the existing design methods outlined in Section 3, the number of experimental results leading to an unconservative evaluation decreased; however, some results prompt an evaluation on the unconservative side within the range of larger width-to-thickness ratios. Therefore, the ratio between the diameter of the bolt hole and the connected leg (d/b), which is a factor affecting the efficiency of the connection, is reflected in the design equation for ultimate tensile strength. Figure 15A displays the ultimate tensile strength trend as a function of the reduction factor U' for each value of $\sqrt{e_x{}^2+e_y{}^2}/L$. The results presented in Figure 15A are the FEA outcomes discussed in Section 4.

In Figure 15A, a reduction factor β is established according to the ratio of the bolt hole diameter to the connected leg (d/b), wherein the evaluation value $P_{u,e}/S_u'$—calculated with the

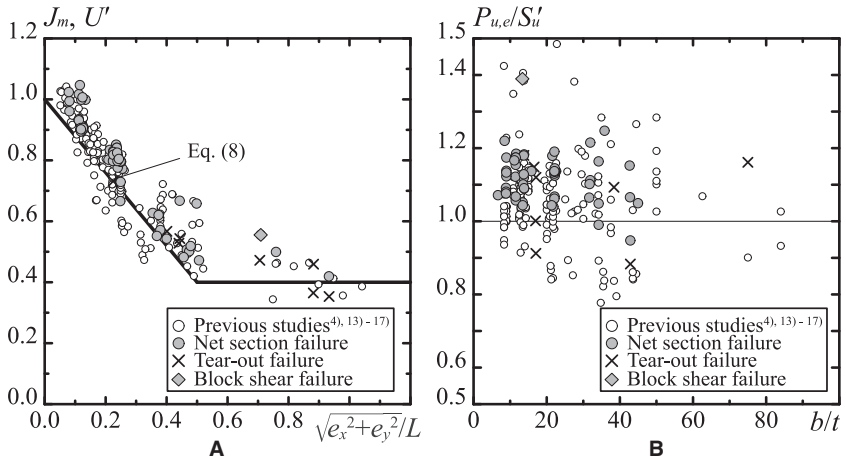

FIGURE 14 Comparisons between shear lag factor U' and test results: (A) J_m versus $\sqrt{e_x{}^2+e_y{}^2}/L$, and (B) $P_{u,e}/S_u'$ versus b/t

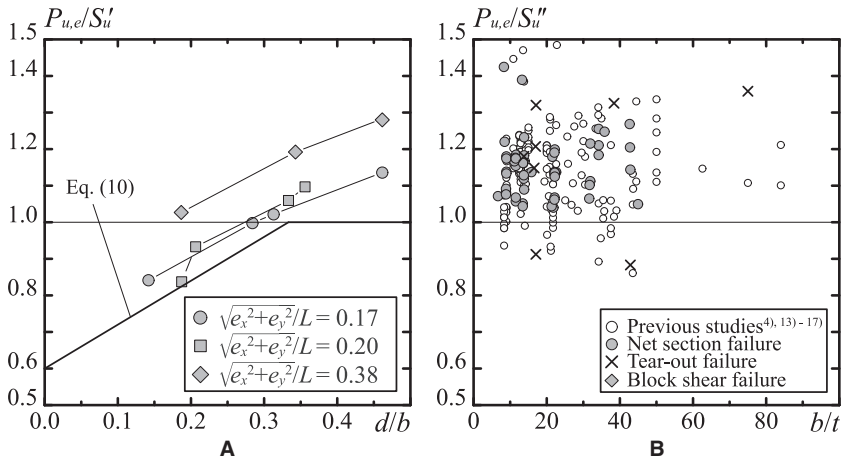

FIGURE 15 Comparisons between shear lag factor U'' and test results: (A) $P_{u,e}/S_u'$ versus d/b, and (B) $P_{u,e}/S_u''$ versus b/t

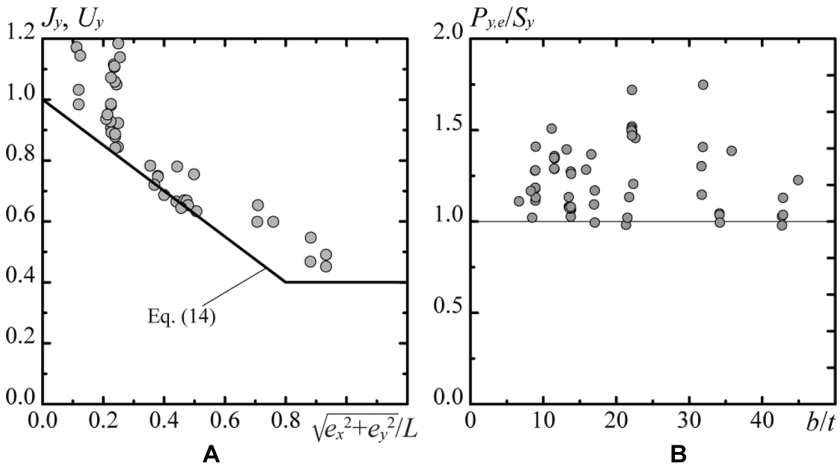

FIGURE 16 Comparisons between the shear lag factor U_y and test results: (A) J_y versus $\sqrt{e_x^2 + e_y^2}/L$, and (B) $P_{y,e}/S_y$ versus b/t

shear lag factor U'—is <1.0 and the evaluation falls on the unconservative side.

$$\beta = \begin{cases} 0.6 + 1.2\dfrac{d}{b} \text{ for } 0.0 \le d/b < 0.33 \\ 1.0 \text{ for } 0.33 \le d/b \end{cases}. \quad (10)$$

The ultimate tensile strength S_u'' computed using the reduction factor β, predicated on the ratio of the bolt hole diameter to the connected leg (d/b) as per Equation (11), aligns with the experimental results depicted in Figure 15B.

$$U'' = \beta\left(1 - 1.2\frac{\sqrt{e_x^2 + e_y^2}}{L}\right), \quad (11)$$

$$S_u'' = U''A_n\sigma_u\,. \quad (12)$$

Compared with the current design methods outlined in Section 3, the scatter of the evaluation results based on Equations (11) and (12) is smaller. Furthermore, the evaluation results derived from the proposed design equation (Equation (12)) were conservative, regardless of the width-to-thickness ratio, thus validating the proposed design equation's efficacy. Although the design equation for the ultimate tensile strength of bolted connections, demonstrated in Equations (10)–(12), lacks a term for the width-to-thickness ratio (b/t), the effects of plate thickness t in the eccentric distance, and the effect of cross-sectional width b on the ratio of the bolt hole diameter to the connected leg (d/b) are incorporated. Therefore, the proposed design equations can be used to indirectly assess the effect of the width-to-thickness ratio (b/t). Thus, Equations (10)–(12) can serve as the unified design equations for the ultimate tensile strength of bolted connections for both thin and thick members.

5.2 Design equation for yield tensile strength

Finally, the design equations for the yield tensile strength of the bolted connections were deduced. Owing to the absence of yield tensile strength reporting in earlier studies, the design equations were developed exclusively from the tests conducted in this research. The yield connection efficiency J_y, defined as the ratio of the yield tensile strength $P_{y,e}$ to the yield axial force P_y predicated on the net area excluding the bolt holes, can be expressed as in Equation (13).

$$J_y = \frac{P_{y,e}}{A_n\sigma_y}. \quad (13)$$

Figure 16A shows the yield connection efficiency J_y on the vertical axis and $\sqrt{e_x^2 + e_y^2}/L$ on the horizontal axis. Similar to the connection efficiency J_m shown in Figure 14A, the yield connection efficiency J_y decreases when $\sqrt{e_x^2 + e_y^2}/L$ increases; thus, the yield connection efficiency J_y can be evaluated by $\sqrt{e_x^2 + e_y^2}/L$. The reduction ratio U_y for the yield tensile strength was set as shown in Equation (14), and the design equation of the bolted connections for the yield strength was evaluated using Equation (15).

$$U_y = \begin{cases} 1 - 0.75\dfrac{\sqrt{e_x^2 + e_y^2}}{L} \text{ for } 0.0 \le \sqrt{e_x^2 + e_y^2}/L < 0.8 \\ 0.4 \text{ for } 0.8 \le \sqrt{e_x^2 + e_y^2}/L \end{cases}, \quad (14)$$

$$S_y = U_yA_n\sigma_y. \quad (15)$$

Figure 16A shows the correlation between Equation (14) and the yield connection efficiency J_y, whereas Figure 16B shows the correlation between the calculated yield tensile strength S_y, which is based on the shear lag factor U_y for the yield tensile strength, and the experimental results from this study. These outcomes signify that the yield strength evaluation results for all specimens are conservative, with a smaller deviation compared with that in the current Japanese standard[5] as illustrated in Figure 6A.

6. Conclusion

In this study, tensile tests and FEA of bolted connections were performed to investigate the tensile strength of brace connections with asymmetric thin-plate members with asymmetric cross sections, such as angle or channel members with a thickness of 6.0 mm or less. The effect of member geometry on the tensile strength of bolted connections was clarified, and unified design equations, applicable to both thin and thick plates, were proposed for evaluating the tensile strength of these connections. The conclusions derived from this study are as follows.

Regardless of variations in the number of bolts and distance between bolt holes, it is observed that the ultimate tensile strength of the bolted connections remains consistent for connections with the same connection length. Furthermore, it was found that the connection efficiency increases with longer connection lengths. Therefore, the current Japanese bolted connection design formula, which relies on the number of bolts as the design variable, proves inadequate in accurately estimating the ultimate tensile strength. Consequently, when evaluating experimental results within the range of relatively large width-to-thickness ratios, particularly when the width-to-thickness ratio exceeds 20, there is a tendency to overestimate the results when employing the current Japanese formula. On the other hand, the design formula of the 2012 edition of the AISI provision based on the shear lag factor U with the ratio of eccentricity ex and joint length L as design variables is more rational than the AIJ design formula and has less tendency to overestimate the experimental results.

Reliable design equations for the ultimate tensile strength are proposed using the combination variable of the eccentric distances (e_x, e_y) in two directions, the connection length and the ratio of the bolt hole diameter to the connected leg width. These proposed design equations provide a reasonable evaluation of the connection of brace members that occur in net section failures from thin to thick plates, and prove to be more effective than existing design equations. Furthermore, the validity of the proposed design equations has been substantiated through comparison with experimental results.

Acknowledgments

This work was supported by JSPS KAKENHI (grant number JP20H2294).

Disclosure

The authors declare that they have no conflicts of interest.

Data Availability Statement

All information and data are given in the text completely.

References

1 National Research Institute for Earth Science and Disaster Prevention: Miyagi Prefecture Offshore Earthquake Disaster Survey Report in 1978; 1978.
2 Ministry of Construction, Building Research Institute: Kobe Earthquake Damage Survey Final Report in 1996; 1996.
3 Kato B, Tanuma Y, Morita K. Research on the brace joints of steel angle with high strength bolts. *Trans Archit Inst Jpn*. 1983;**3**(325):32-39. (in Japanese). doi:10.3130/aijsaxx.325.0_32
4 Kato B, Morita K, Tanuma T. Experimental studies on the strength of brace-to-gusset plate connections with high strength bolts. *Pacific Structural Steel Conference 1st*, 1985;23-37.
5 Architectural Institute of Japan: AIJ Recommendation for Design of Connections in Steel Structures; 2012. (in Japanese).
6 Architectural Institute of Japan: Recommendation for the Design and Fabrication of Light Weight Steel Structures; 2002. (in Japanese).
7 Architectural Institute of Japan: Guidebook on Design and Fabrication of High Strength Bolted Connections; 2016.
8 Munse WH, Chesson E. Riveted and bolted joints: net section design. *J Struct Div*. 1963;**89**(1):107-126. doi:10.1061/JSDEAG.0000869
9 Pan CL. Prediction of the strength of bolted cold-formed channel sections in tension. *J Thin-Walled Struct*. 2004;**42**(8):1177-1198. doi:10.1016/j.tws.2004.02.001
10 Teh LH, Gilbert BP. Net section tension capacity of bolted connections in cold-reduced steel sheets. *J Struct Eng*. 2013;**139**(3):740-747. doi:10.1061/(ASCE)ST.1943-541X.0000477
11 Teh LH, Gilbert BP. Net section tension capacity of cold-reduced sheet steel angle braces bolted at one leg. *J Struct Eng*. 2012;**138**(3):740-747. doi:10.1061/(ASCE)ST.1943-541X.0000675
12 AISI: North American Specification for the Design of Cold-Formed Steel Structural Members 2012 Edition; 2013.
13 Tanaka A, Narihara H, Aoki H. Experimental Study on the Connections of Steel Channel Braces, Summaries of Technical Papers of Annual Meeting, Architectural Institute of Japan; 1983:1319-1320. (in Japanese).
14 Yip AS, Cheng JJR. *Shear Lag in Bolted Cold-Formed Steel Angles and Channels in Tension, Structural Engineering Report 133*. University of Alberta; 2000. doi:10.7939/R3J09WD3T
15 LaBouble RA, Yu WW. *Tensile and Bearing Capacities of Bolted Connections, Final Summary Report, Civil Engineering Study 95–6*. University of Missouri-Rolla; 1995.
16 Paula VF, Bezerra LM, Matias WT. Efficiency reduction due to shear lag on bolted cold-formed steel angles. *J Constr Steel Res*. 2008;**64**:571-583. doi:10.1016/j.jcsr.2007.10.008
17 Tatsumi N, Kishiki S. Effects of connection detail on strength and cyclic deformation capacity of angle brace. *J Struct Constr Eng (Trans AIJ)*. 2017;**82**(736):909-919. (in Japanese). doi:10.3130/aijs.82.909
18 AISI: North American Specification for the Design of Cold-Formed Steel Structural Members 2016 Edition; 2016.
19 American Institute of Steel Construction: Seismic Provisions for Structural Steel Buildings; 2016.
20 CEN Brussels: EN 1993-1-8. Eurocode 3—Design of Steel Structures. Part 1–8, Design of Joints; 2005.
21 Kuwamura H, Yamamoto K. Criterion for ductile crack initiation in structural steels under triaxial stress state. *J Struct Constr Eng (Trans AIJ)*. 1995;**11**(477):129-135. (in Japanese). doi:10.3130/aijs.60.129_4
22 Totsuka M, Ikarashi K, Okada T. Effect of Bolted Angle Connection under Tensile Force, Summaries of Technical Papers of Annual Meeting, Architectural Institute of Japan, Structures-III; 2018:1069-1070. (in Japanese).

How to cite this article: Nagasato K, Ikarashi K, Mitsui K. Strength of bolted steel structural members under eccentric tension. *Jpn Archit Rev*. 2023;6:e12409. https://doi.org/10.1002/2475-8876.12409

Appendix A: List of Test Specimens and Coupon Test Results

Table A1 summarizes the results of the coupon tests described in Section 2, and Table A2 summarizes the specimens for the brace connection tensile tests performed in this study. The M tags in Table A1 correspond to the specimens presented in Table A2. The members in the Size column of Table A2 are the cross-sectional shapes used for the test specimens, where L stands for angle member, C for channel member, and FB for a flat plate. Table A3 lists the test specimens from previous studies.[4,13–17] The ultimate strength $P_{u,b,c}$ determined by the

TABLE A1 Material properties

t	M tag.	E [GPa]	σ_y [MPa]	σ_u [MPa]	$Y.R.$ [%]	ε_u [%]	ε_f [%]
1.6	a	160	158	294	54.1	36.2	41.3
2.3	b	173	157	293	53.6	34.2	43.8
2.3	c	209	282	440	64.1	24.7	32.8
2.3	d	206	312	430	72.6	35.3	38.7
3.2	e	183	188	302	62.3	30.4	44.4
4.0	f	205	339	470	73.4	23.0	32.4
4.5	g	186	203	319	63.6	35.4	41.1
4.5	h	202	217	340	63.8	27.5	30.2
6.0	i	212	301	453	66.4	21.5	24.3
6.0	j	206	310	455	68.1	26.4	29.3
6.0	k	216	332	457	72.6	34.3	38.0
8.0	l	205	307	454	67.6	22.8	33.4

Note: M tag in this table corresponds to M tag in Table A2.

TABLE A2 List of specimens and test results in this study

No.	Size	M tag	l [mm]	e_1 [mm]	e_2 [mm]	t_{GP} [mm]	d [mm]	n [−]	p [mm]	L [mm]	$P_{y,e}$ [kN]	$P_{u,b,c}$ [kN]	$P_{u,e}$ [kN]	δ_u [mm]	J_m [−]
1	L-50 × 50 × 1.6	a	700	30	25	3.2	17	3	40	80	23.3	33.6	29.3	31.21	0.772
2	L-50 × 50 × 2.3	b	700	30	25	4.5	17	3	40	80	33.6	48.2	42.1	28.27	0.797
3	L-50 × 50 × 3.2	e	700	30	25	6.0	17	3	40	80	50.3	69.1	61.5	26.47	0.805
4	L-50 × 50 × 4.0※	f	700	30	25	9.0	17	3	40	80	83.7	134.4	105.1	16.32	0.776
5	L-50 × 50 × 4.5	g	700	30	25	9.0	17	3	40	80	74.5	102.6	91.3	26.79	0.825
6	L-50 × 50 × 6.0※	i	700	30	25	12	17	3	40	80	126.9	194.3	157.6	21.98	0.798
7	L-50 × 50 × 8.0※	l	700	30	25	16	17	3	40	80	163.0	259.7	204.1	21.44	0.802
8	L-50 × 50 × 2.3	b	700	30	25	4.5	17	5	40	160	40.0	75.1	48.9	37.62	0.907
9	L-50 × 50 × 4.0※	f	700	30	25	9.0	17	5	40	160	104.1	209.6	123.9	21.45	0.901
10	L-50 × 50 × 4.5	g	700	30	25	9.0	17	5	40	160	86.5	160.1	100.4	30.00	0.906
11	L-50 × 50 × 6.0※	i	700	30	25	12	17	5	40	160	160.3	303.1	184.1	36.57	0.931
12	L-50 × 50 × 2.3	b	700	30	25	4.5	17	3	80	160	39.6	75.1	48.6	43.74	0.902
13	L-50 × 50 × 4.0※	f	700	30	25	9.0	17	3	80	160	99.4	209.6	123.1	18.21	0.895
14	L-50 × 50 × 4.5	g	700	30	25	9.0	17	3	80	160	86.8	160.1	100.8	32.94	0.916
15	L-50 × 50 × 6.0※	i	700	30	25	12	17	3	80	160	161.0	303.1	185.5	37.33	0.935
16	L-50 × 50 × 2.3	b	700	30	25	9.0	17	3	40	80	35.3	48.2	42.8	29.86	0.795
17	L-50 × 50 × 4.0※	f	700	30	25	19	17	3	40	80	87.6	134.4	108.3	15.61	0.798
18	L-50 × 50 × 4.5	g	700	30	25	19	17	3	40	80	78.1	102.6	93.0	22.59	0.841
19	L-50 × 50 × 6.0※	i	700	30	25	25	17	3	40	80	134.5	194.3	163.8	18.33	0.827
20	L-50 × 75 × 2.3	b	700	30	25	4.5	17	3	40	80	–	48.2	44.0	28.19	0.621
21	L-50 × 25 × 2.3	b	700	30	25	4.5	17	3	40	80	31.3	48.2	37.5	38.92	0.999
22	L-50 × 25 × 4.0※	f	700	30	25	9.0	17	3	40	80	78.6	134.4	94.2	13.58	1.007
23	L-50 × 25 × 4.5	g	700	30	25	9.0	17	3	40	80	66.9	102.6	76.4	25.35	0.999
24	L-50 × 25 × 6.0※	i	700	30	25	12	17	3	40	80	121.0	194.3	137.5	33.75	1.017
25	L-50 × 20 × 1.6	a	700	30	25	3.2	17	3	40	80	20.8	33.6	25.2	38.13	1.047
26	L-50 × 50 × 2.3	b	700	30	25	4.5	13	3	40	80	37.3	49.5	46.1	36.92	0.816
27	L-50 × 50 × 4.0	f	700	30	25	9.0	13	3	40	80	94.0	138.2	115.2	22.31	0.802
28	L-50 × 50 × 4.5	g	700	30	25	9.0	13	3	40	80	79.6	105.5	95.4	29.86	0.819
29	L-50 × 50 × 6.0※	i	700	30	25	12	13	3	40	80	136.8	199.8	173.3	29.46	0.835
30	L-50 × 50 × 2.3	b	380	30	25	4.5	17	3	40	80	35.2	48.2	42.8	27.66	0.795
31	L-50 × 50 × 4.0※	f	380	30	25	9.0	17	3	40	80	87.6	134.4	108.3	18.09	0.805
32	L-50 × 50 × 4.5	g	380	30	25	9.0	17	3	40	80	78.1	102.6	93.0	23.17	0.841
33	L-50 × 50 × 6.0※	i	380	30	25	12	17	3	40	80	134.6	194.3	163.8	20.36	0.831
34	C-50 × 30 × 1.6	a	700	30	25	9.0	17	3	40	80	24.5	51.7	41.9	19.87	0.994
35	C-50 × 30 × 2.3	b	700	30	25	9.0	17	3	40	80	44.3	74.1	60.9	18.23	1.024
36	C-50 × 30 × 10 × 1.6	a	700	30	25	9.0	17	3	40	80	33.2	51.7	48.3	21.16	0.961
37	FB-50 × 2.3	b	700	30	25	9.0	17	3	40	80	12.4	74.1	26.4	15.61	1.191
38	FB-50 × 6.0	i	700	30	25	9.0	17	3	40	80	61.0	299.0	92.2	13.68	1.050
39	L-100 × 100 × 2.3	c	700	30	50	12	17	3	40	80	80.0	97.7	94.6	29.82	0.507
40	L-80 × 80 × 2.3	c	700	30	40	12	17	3	40	80	69.6	87.5	83.1	23.84	0.572
41	L-100 × 100 × 6.0	j	700	30	50	16	17	3	40	80	207.8	263.4	248.1	28.12	0.528
42	L-80 × 80 × 6.0	j	700	30	40	16	17	3	40	80	187.6	236.1	226.2	24.43	0.627
43	L-50 × 50 × 2.3	c	700	30	25	9.0	17	3	40	80	48.2	72.4	59.5	14.25	0.729
44	L-50 × 50 × 4.5	h	700	30	25	9.0	17	3	40	80	82.2	109.4	98.4	19.66	0.852
45	L-50 × 80 × 2.3	c	700	30	25	12	17	3	40	80	50.1	72.4	61.7	15.27	0.543
46	L-50 × 100 × 2.3	c	700	30	25	12	17	3	40	80	54.7	72.4	63.6	14.73	0.472
47	L-80 × 100 × 2.3	c	700	30	40	12	17	3	40	80	70.9	87.5	83.2	25.09	0.502
48	L-100 × 50 × 2.3	c	700	30	50	9	17	3	40	80	72.6	97.7	89.4	30.71	0.666
49	L-50 × 100 × 6.0	j	700	30	25	16	17	3	40	80	147.0	195.2	175.6	18.10	0.519
50	L-100 × 50 × 6.0	j	700	30	50	12	17	3	40	80	203.6	263.4	246.7	33.41	0.731
51	L-80 × 80 × 2.3	c	700	30	40	12	13	3	40	80	69.0	89.6	82.6	26.59	0.552
52	L-100 × 100 × 2.3	c	700	30	50	12	13	3	40	80	78.8	99.7	92.1	28.59	0.482
53	L-100 × 100 × 2.3	c	800	30	50	16	17	2	40	40	53.9	77.4	65.7	19.87	0.353
54	L-100 × 100 × 6.0	j	800	30	50	16	17	2	40	40	146.0	208.8	171.5	18.23	0.365
55	L-80 × 80 × 6.0	j	800	30	40	16	17	2	40	40	143.4	181.5	170.0	21.16	0.472
56	L-100 × 100 × 2.3	d	800	40	50	16	17	2	40	40	61.6	80.6	72.6	22.74	0.420
57	L-100 × 100 × 6.0	k	800	40	50	16	17	2	40	40	194.0	223.5	224.2	31.75	0.459
58	L-80 × 80 × 2.3	d	800	40	40	16	17	2	40	40	58.6	70.7	67.4	22.07	0.499

Table A2 (Continued)

No.	Size	M tag	l [mm]	e_1 [mm]	e_2 [mm]	t_{GP} [mm]	d [mm]	n [−]	p [mm]	L [mm]	$P_{y,e}$ [kN]	$P_{u,b,c}$ [kN]	$P_{u,e}$ [kN]	δ_u [mm]	J_m [−]
59	L-80 × 80 × 6.0	k	800	40	40	16	17	2	40	40	179.9	196.1	210.6	26.12	0.556
60	L-50 × 50 × 2.3	d	800	40	25	9.0	17	2	40	40	42.6	55.9	51.1	13.68	0.658
61	L-50 × 50 × 6.0	k	800	40	25	9.0	17	2	40	40	120.7	154.9	142.1	18.72	0.667

Note: Names without ※ represent cold-formed members. Names with ※ represent specimens made by hot roll. M tag in Table A2 corresponds to M tag in Table A1.

TABLE A3 List of specimens and test results from previous studies

Ref. No.	b [mm]	h [mm]	t [mm]	e_1 [mm]	e_2 [mm]	d [mm]	n [−]	p [mm]	e_x [mm]	e_y [mm]	σ_y [MPa]	σ_u [MPa]	$P_{u,e}$ [kN]	$P_{u,e}/P_{u,c}$ [−]	J_m [−]
4	50	50	6.0	30	25	14	5	40	12.1	12.1	361	489	194	0.98	0.83
4	50	50	6.0	30	22	18	5	40	12.7	16.4	348	477	197	1.08	0.91
4	65	65	6.0	30	33	18	5	40	16.4	16.4	339	473	271	1.06	0.90
4	75	75	6.0	30	33	18	5	40	18.9	24.0	301	451	265	0.91	0.78
4	75	75	6.0	30	38	18	5	40	18.9	18.9	301	451	276	0.95	0.81
4	75	75	6.0	30	43	18	5	50	18.9	12.6	301	451	314	1.08	0.92
4	75	75	6.0	30	43	18	5	60	18.9	12.6	317	458	323	1.10	0.93
4	75	75	6.0	30	33	18	4	40	18.9	24.0	301	451	238	0.87	0.70
4	75	75	6.0	30	38	18	4	40	18.9	18.9	301	451	263	0.96	0.77
4	75	75	6.0	30	43	18	4	50	18.9	12.6	301	451	307	1.12	0.90
4	75	75	6.0	30	43	18	4	60	18.9	12.6	301	451	309	1.13	0.91
4	75	75	6.0	35	41	22	5	50	19.5	15.4	301	451	305	1.09	0.92
4	75	75	6.0	35	41	22	4	50	19.5	15.4	301	451	294	1.12	0.89
4	75	75	6.0	35	41	22	3	50	19.5	15.4	305	428	245	1.13	0.78
4	75	75	6.0	40	38	24	4	55	19.8	19.8	301	451	297	1.15	0.91
4	75	75	6.0	40	38	24	3	55	19.8	19.8	301	451	266	1.19	0.82
4	90	90	7.0	35	40	22	5	50	22.8	28.5	359	504	380	0.84	0.71
4	90	90	7.0	35	50	22	5	50	22.8	17.1	357	504	441	0.97	0.83
4	90	90	7.0	35	60	22	5	50	22.8	5.6	357	504	472	1.04	0.89
4	90	90	7.0	35	40	22	4	50	22.8	28.5	314	460	367	0.94	0.75
4	90	90	7.0	35	50	22	4	50	22.8	17.1	359	504	427	1.00	0.80
4	90	90	7.0	35	50	22	4	65	22.8	17.1	357	504	456	1.06	0.86
4	90	90	7.0	35	50	22	4	80	22.8	17.1	359	504	465	1.09	0.87
4	90	90	7.0	40	50	22	4	50	22.8	17.1	359	504	450	1.05	0.84
4	90	90	7.0	40	50	24	5	50	23.1	17.3	357	504	458	1.03	0.87
4	90	90	7.0	40	50	24	5	55	23.1	17.3	359	504	470	1.05	0.89
4	90	90	7.0	40	50	24	4	55	23.1	17.3	359	504	436	1.04	0.83
4	90	90	7.0	40	50	24	4	70	23.1	17.3	357	504	464	1.10	0.88
4	90	90	7.0	40	50	24	4	55	23.1	17.3	357	504	466	1.11	0.89
4	90	90	7.0	40	50	24	3	55	23.1	17.3	314	460	368	1.11	0.77
4	90	90	7.0	45	50	26	4	60	23.4	17.5	359	504	471	1.14	0.91
4	90	90	7.0	45	50	26	3	60	23.4	17.5	357	504	408	1.13	0.79
4	90	90	7.0	45	50	26	3	90	23.4	17.5	357	504	448	1.24	0.86
4	90	90	7.0	45	50	26	3	120	23.4	17.5	325	449	415	1.29	0.90
4	90	90	7.0	60	50	26	2	240	23.4	17.5	325	449	427	1.62	0.92
4	90	90	10	40	40	24	5	55	21.9	27.7	320	474	559	0.95	0.81
4	90	90	10	40	48	24	5	55	21.9	18.4	320	474	627	1.07	0.91
4	90	90	10	40	48	24	4	55	21.9	18.4	320	474	570	1.03	0.82
4	90	90	10	40	48	24	4	55	21.9	18.4	320	474	591	1.07	0.85
4	90	90	10	40	48	24	4	70	21.9	18.4	320	474	603	1.09	0.87
4	90	90	10	40	48	24	4	90	21.9	18.4	320	474	613	1.11	0.88
4	100	100	7.0	35	60	22	5	50	25.3	14.0	348	497	509	1.00	0.86
4	100	100	7.0	35	60	22	4	65	25.3	14.0	348	497	493	1.03	0.83
13	75	40	5.0	55	37.5	18	3	55	12.8	0	321	452	334	1.50	0.93
13	75	40	5.0	40	37.5	18	4	50	12.8	0	321	452	357	1.33	1.00
13	75	40	5.0	40	37.5	18	5	50	12.8	0	321	452	369	1.14	1.03
13	75	40	5.0	40	37.5	18	6	50	12.8	0	321	452	368	1.08	1.03

Table A3 (Continued)

Ref. No.	b [mm]	h [mm]	t [mm]	e_1 [mm]	e_2 [mm]	d [mm]	n [−]	p [mm]	e_x [mm]	e_y [mm]	σ_y [MPa]	σ_u [MPa]	$P_{u,e}$ [kN]	$P_{u,e}/P_{u,c}$ [−]	J_m [−]
13	75	40	5.0	80	37.5	22	2	80	12.8	0	321	452	305	1.65	0.87
13	75	40	5.0	60	37.5	22	3	60	12.8	0	321	452	349	1.52	1.00
13	75	40	5.0	50	37.5	22	4	60	12.8	0	321	452	364	1.22	1.04
13	100	50	5.0	75	50	22	3	75	15.4	0	323	457	429	1.46	0.87
13	100	50	5.0	50	50	22	4	60	15.4	0	323	457	458	1.39	0.93
13	100	50	5.0	50	50	22	5	60	15.4	0	323	457	477	1.20	0.97
13	100	50	5.0	50	50	22	6	60	15.4	0	323	457	485	1.04	0.98
13	100	50	5.0	110	50	26	2	110	15.4	0	323	457	384	1.57	0.79
13	100	50	5.0	75	50	26	3	75	15.4	0	323	457	466	1.60	0.96
13	100	50	5.0	60	50	26	4	70	15.4	0	323	457	480	1.34	0.99
13	100	50	5.0	60	50	26	5	70	15.4	0	323	457	497	1.13	1.02
13	125	65	6.0	90	62.5	26	3	90	19	0	338	468	644	1.48	0.88
13	125	65	6.0	70	62.5	26	4	70	19	0	338	468	689	1.45	0.95
13	125	65	6.0	60	62.5	26	5	70	19	0	338	468	731	1.27	1.00
14	76	76	1.2	21	38	21	3	63.5	21.6	21.6	277	317	38	1.08	0.76
14	102	102	1.2	21	51	21	3	63.5	27.9	27.9	277	317	45	0.98	0.64
14	102	102	1.2	21	51	21	4	63.5	27.9	27.9	277	317	49	0.86	0.70
15	41	41	1.1	51	21	15	2	38.1	12.1	12.1	247	385	16	0.98	0.56
15	41	41	1.1	51	21	15	3	38.1	12.1	12.1	247	385	20	1.02	0.71
15	41	41	3.0	51	21	15	2	38.1	11.3	11.3	252	366	49	1.24	0.69
15	41	41	3.0	51	21	15	3	38.1	11.3	11.3	252	366	59	1.20	0.82
15	41	83	1.1	51	21	15	2	38.1	30.7	15.1	247	385	18	0.90	0.39
15	41	83	1.1	51	21	15	3	38.1	30.7	15.1	247	385	22	0.79	0.49
15	83	41	1.1	51	41	15	2	38.1	7.5	15.1	247	385	25	0.86	0.54
15	83	41	1.1	51	41	15	3	38.1	7.5	15.1	247	385	30	0.82	0.66
15	41	83	3.0	51	21	15	2	38.1	29.8	14.3	252	366	54	1.04	0.46
15	41	83	3.0	51	21	15	3	38.1	29.8	14.3	252	366	62	0.86	0.53
15	83	41	3.0	51	41	15	2	38.1	6.9	14.3	252	366	80	1.08	0.69
15	83	41	3.0	51	41	15	3	38.1	6.9	14.3	252	366	90	0.95	0.77
16	50	50	2.2	35	25	14	2	38.1	13.7	13.7	–	502	55	1.02	0.59
16	50	50	2.3	35	25	14	3	38.1	13.6	13.6	–	502	65	0.97	0.68
16	50	50	2.3	35	25	14	4	38.1	13.6	13.6	–	502	78	0.99	0.80
16	50	50	3.5	35	25	14	2	38.1	13.1	13.1	–	463	89	1.16	0.67
16	50	50	3.5	35	25	14	3	38.1	13.1	13.1	–	463	98	1.06	0.73
16	50	50	3.6	35	25	14	4	38.1	13.1	13.1	–	463	102	0.94	0.75
16	50	50	3.7	35	25	14	2	38.1	13.1	13.1	–	457	82	1.03	0.59
16	50	50	3.7	35	25	14	3	38.1	13.0	13.0	–	457	97	1.00	0.70
16	50	50	3.7	35	25	14	4	38.1	13.1	13.1	–	457	110	1.00	0.80
16	80	80	2.4	35	40	14	3	38.1	21.0	21.0	–	502	94	0.91	0.54
16	80	80	2.3	35	40	14	4	38.1	21.1	21.1	–	502	92	0.77	0.56
16	80	80	3.5	35	40	14	2	38.1	20.5	20.5	–	463	108	0.99	0.46
16	80	80	3.6	35	40	14	3	38.1	20.5	20.5	–	463	131	0.92	0.56
16	80	80	3.7	35	40	14	4	38.1	20.5	20.5	–	463	142	0.80	0.59
16	80	80	3.9	35	40	14	2	38.1	20.4	20.4	–	457	115	0.98	0.46
16	80	80	3.8	35	40	14	3	38.1	20.4	20.4	–	457	140	0.94	0.57
16	80	80	3.8	35	40	14	4	38.1	20.5	20.5	–	457	143	0.79	0.59
16	100	100	2.3	35	50	14	3	38.1	26.0	26.0	–	502	110	1.02	0.53
16	100	100	2.6	35	50	14	4	38.1	25.9	25.9	–	502	115	0.78	0.49
16	100	100	3.5	35	50	14	2	38.1	25.5	25.5	–	463	122	1.03	0.41
16	100	100	3.5	35	50	14	3	38.1	25.5	25.5	–	463	152	0.98	0.52
16	100	100	3.7	35	50	14	4	38.1	25.5	25.5	–	463	165	0.84	0.53
16	100	100	3.9	35	50	14	3	38.1	25.4	25.4	–	457	161	0.94	0.49
16	100	100	3.9	35	50	14	4	38.1	25.4	25.4	–	457	179	0.88	0.56
16	50	80	2.4	35	25	14	2	38.1	26.5	16.3	–	502	62	0.99	0.45
16	50	80	2.4	35	25	14	3	38.1	26.5	16.3	–	502	71	0.82	0.51
16	50	80	2.4	35	25	14	4	38.1	26.6	16.3	–	502	78	0.76	0.58
16	50	100	2.5	35	25	14	2	38.1	35.7	17.4	–	502	64	0.99	0.39

Table A3 (Continued)

Ref. No.	b [mm]	h [mm]	t [mm]	e_1 [mm]	e_2 [mm]	d [mm]	n [–]	p [mm]	e_x [mm]	e_y [mm]	σ_y [MPa]	σ_u [MPa]	$P_{u,e}$ [kN]	$P_{u,e}/P_{u,c}$ [–]	J_m [–]
16	50	100	2.6	35	25	14	3	38.1	35.6	17.3	–	502	77	0.83	0.44
16	50	100	2.4	35	25	14	4	38.1	35.7	17.4	–	502	82	0.76	0.51
16	80	100	2.3	35	40	14	2	38.1	29.2	23.2	–	502	69	0.87	0.36
16	80	100	2.3	35	40	14	3	38.1	29.2	23.2	–	502	81	0.80	0.42
16	80	100	2.3	35	40	14	4	38.1	29.2	23.2	–	502	89	0.74	0.47
16	80	50	2.3	35	40	14	2	38.1	10.0	16.3	–	502	67	0.87	0.51
16	80	50	2.3	35	40	14	3	38.1	10.0	16.3	–	502	78	0.79	0.60
16	80	50	2.2	35	40	14	4	38.1	10.0	16.4	–	502	85	0.78	0.67
16	100	50	2.3	35	50	14	3	38.1	8.5	17.5	–	502	90	0.83	0.59
16	100	50	2.3	35	50	14	4	38.1	8.5	17.5	–	502	103	0.78	0.67
17	65	65	6.0	40	33	18	2	60	16.4	16.4	320	444	204	1.27	0.72
17	65	65	6.0	40	33	18	3	60	16.4	16.4	320	444	243	1.24	0.86
17	65	65	6.0	40	33	18	4	60	16.4	16.4	320	444	258	1.15	0.91
17	65	65	6.0	40	33	18	5	60	16.4	16.4	320	444	267	1.12	0.95

block shear failure was calculated based on design equations in AIJ Recommendation for Design of Connections in Steel Structures,[5] as follows.

$$P_{u,b,c} = (A_{nt} + 0.5A_{ns})\sigma_u, \tag{A1}$$

where A_{nt} is the area where tensile force acts, and A_{st} is the area where shear forces act.

Appendix B: Definition of Yield Tensile Strength

The yield tensile strength is defined as the intersection of dashed lines A and B, as shown in Figure A1.[22] Dashed line A is a straight line connecting the ultimate tensile strength $P_{u,e}$ and $0.9P_{u,e}$ (90% of the ultimate tensile strength), whereas dashed line B is a straight line connecting $0.3P_{u,e}$ (30% of the ultimate tensile strength) and $0.5P_{u,e}$ (50% of the ultimate tensile strength).

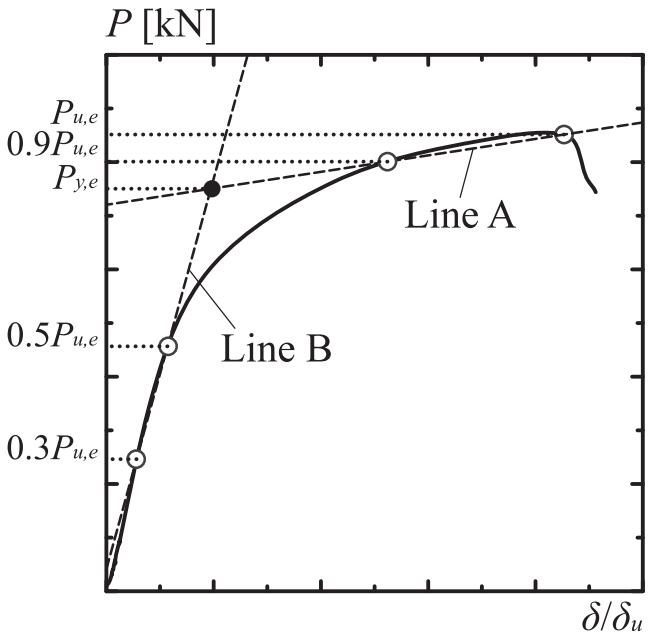

FIGURE A1 Definition of yield tensile strength

Appendix C: Comparisons of Experimental Results with Design Equations for Brace Connections in AISI, AISC, and Eurocode 3

Appendix C compares the experimental results with the ultimate tensile strength based on the design equations for brace connections in the 2016 edition of AISI[18,19] and Eurocode 3,[20] which are not presented in Section 3. In the United States, steel members with a plate thickness of 4.76 mm or less are designed using the design equations of the North American Specification for the Design of Cold-formed Steel Structural Members 18), whereas members thicker than 4.76 mm are designed using the design equations provided in the Seismic Provisions for Structural Steel Buildings.[19] In the 2012 edition of the AISI provisions, the same design equations are used to calculate the tensile strength of bolted and welded connections. However, in the 2016 edition, bolted and welded connections are classified and provide separate design equations. Figure A2A shows a comparison of the test results and calculations based on the 2016 edition of the AISI provision. Figure A2B shows a comparison of the test results and calculations based on the design equations provided in the 2016 edition of the AISC provision for plate thicknesses >4.76 mm. The vertical axes in Figure A2A,B are normalized by calculations based on the 2016 edition of the AISI provision $s_{u.AISI2016}$ and the 2016 edition of the AISC provision $s_{u.AISC2016}$, respectively. The 2016 edition of the AISI provision for relatively thin plates shows a good correspondence between the experimental and calculation results in the range of width-to-thickness ratios >40, whereas the 2016 edition of the AISC provision for relatively thick plates shows a good correspondence in the range of width-to-thickness ratios <30. However, a large scatter exists, and neither design equation provides a unified design procedure for both thin and thick plate members. The Eurocode design equation shown in Figure A2C is expressed in terms of a reduction factor that considers the number of bolts and bolt pitch. However, the calculation results based on the design equation in Eurocode 3 also exhibit a large scatter, with smaller width-to-thickness ratios, thus resulting in overly conservative assessments.

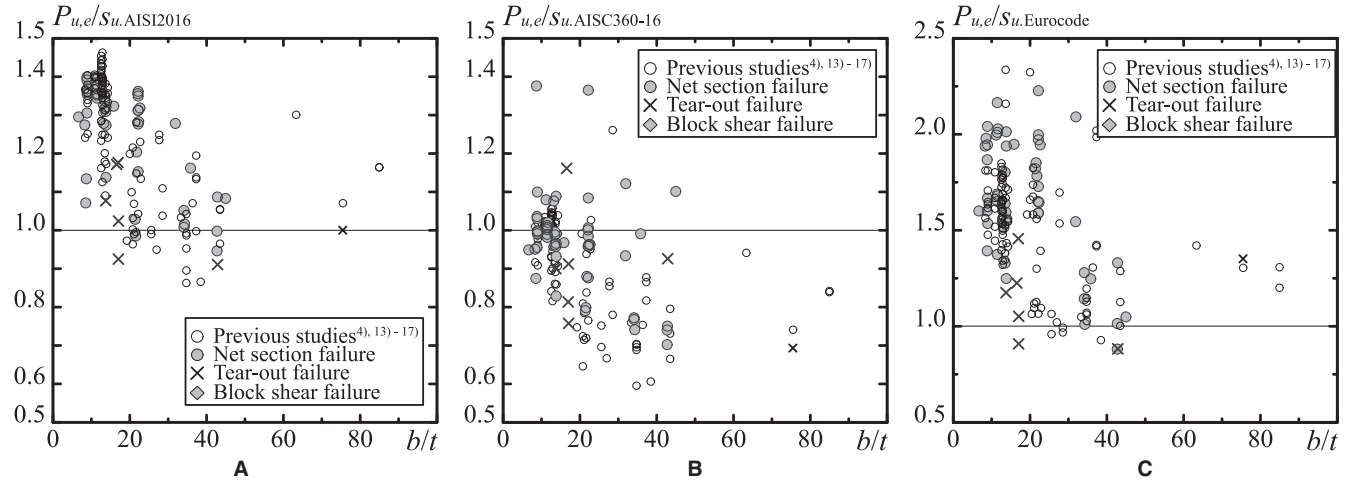

FIGURE A2 Comparisons between tensile test results and calculations in several design provisions: (A) 2016 edition of the AISI, (B) 2016 edition of the AISC, and (C) Eurocode 3